# Electric Field Grading and Discharge Inception Voltage Improvement on HVDC GIS/GIL Spacer with Permittivity and Conductivity Graded Materials ($\varepsilon/\sigma$-FGM)

Rachmawati, Hiroki Kojima, Katsumi Kato, Nabila Zebouchi, and Naoki Hayakawa

***Abstract*—Functionally graded materials (FGM) application with graded permittivity and conductivity is promising as an effective technique for electric field relaxation in $SF_6$ gas around HVDC GIS/GIL spacers. In order to approach the practical application of FGM to HVDC GIS/GIL spacers, this paper investigates the electric field reduction effect given by permittivity and conductivity graded materials (ε/σ-FGM) based on actual measured permittivity (ε) characteristics of $SrTiO_3$-filled epoxy composites and conductivity (σ) characteristics of SiC-filled epoxy composites. In addition, theoretical discharge inception voltage (TDIV) of ε/σ-FGM spacer is calculated under standard lightning impulse (LI) voltage based on the Volume-Time theory. The results show that ε/σ-FGM spacer with grading to lower permittivity (GLP) ($\varepsilon_r$ from 12.7 to 4) containing 0 to 26.9 vol% $SrTiO_3$-filled epoxy composite and U-shaped graded conductivity containing 5 to 10 vol% SiC-filled epoxy composite is effective for electric field relaxation under DC steady state (DC-SS) and LI voltage where both resistive and capacitive fields present. It is attributed to the higher ε and σ of FGM spacer near the HV conductor/spacer interface. TDIV under LI voltage is also estimated to be 26% higher at 0.5 MPa-abs, compared to the conventional spacer without ε/σ-grading.**

***Index Terms*—breakdown voltage, conductivity, electric field grading, functionally graded materials (FGM), permittivity**

## I. Introduction

THE growth on demand of HVDC transmission system utilization has been increasing over the last few decades owing to the high transmission efficiency, large capacity, and low losses, so that it is advantageous for interconnection grids among distributed power generations as well as for electricity trading between countries. These purposes have encouraged research and investigations on improving the reliability of the DC apparatus. While DC apparatus such as gas insulated switchgear (GIS) and gas insulated transmission lines (GIL) are favorable due to the compactness which is economical as well as environmentally friendly, they have shortcomings where local electric field is enhanced as a result of charge accumulation under DC stress, especially at the contacts of three different materials (Conductor (HV/GND), solid insulator (spacer), and $SF_6$ gas, also called as triple junction (TJ)). Moreover, the conductivity of the insulating material is also influenced by the temperature as well as by the electric field, causing further enhanced fields around the TJ. This continuous exposure to high field stress can accelerate the aging which eventually leads to insulation failures [1-4].

Some attempts to control the electric fields have been conducted by modifying the structure of either the spacer or the conductor, whereas some others prefer modifying the material properties of the spacer for the purpose of electric field grading [5]. In the last few decades, many researchers have started the development of field grading materials with non linear permittivity/ε (for AC applications) and/or conductivity/σ (for DC applications) to insulators in order to reduce the high field stress at critical points. Pradhan *et al* have investigated the conductivity characteristics of SiR-based field grading materials doped with various concentrations of ZnO microvaristors for different insulator applications [6]. Du *et al* fabricated a DC GIL spacer coated with functionally graded ZnO film by stratified magnetron sputtering method which can improve the electric field distribution, hence improved the DC flashover voltage by 17.4% under negative voltage compared to the conventional spacer [7]. X. Li *et al* have fabricated a conductivity non-uniform insulator using 3D printing method, where the DC flashover voltages have considerably improved at various $SF_6$ gas pressures [8]. C. Li *et al* combined both shape and material optimizations in HVDC charge adaptive control spacer (CACS) made of SiC-doped epoxy/$Al_2O_3$ composite by

This work was supported by JSPS KAKENHI Grant Number JP18H01423 and by the Hibi Science Foundation. *Corresponding author: Rachmawati.*

Rachmawati, Hiroki Kojima, and Naoki Hayakawa are with the Department of Electrical Engineering, Nagoya University, Furo-cho, Chikusa-ku, Nagoya 464-8603, Japan (e-mail: rachmawati@hayakawa.nuee.nagoya-u.ac.jp, kojima@nuee.nagoya-u.ac.jp, nhayakaw@nuee.nagoya-u.ac.jp).

Katsumi Kato is with the Department of Electrical Engineering and Information Science, National Institute of Technology, Niihama College, 7-1 Yaguma-cho, Niihama 792-8580, Japan (e-mail: k.kato@niihama-nct.ac.jp )

Nabila Zebouchi is with the Advanced High Voltage Engineering Research Centre, Cardiff University, Cardiff CF24 3AA, UK (e-mail: ZebouchiN@cardiff.ac.uk)

dividing the volume into two regions, i.e. the insulation region and the charge adaptive control region with different doping ratio to reduce the surface potential and improve the DC surface flashover voltage [1,9].

Most of the above field grading materials are applied in the form of surface coating or thin film, while the application to bulk insulator is still limited. The 3D printing method is one way to produce bulk insulator, however it still has problems such as voids which may reduce the mechanical and electrical strength, and a limited range of filler contents may result in relatively smaller range of ε grading, hence lower field reduction [8,10]. Moreover, most of their field grading effect would rely on the nonlinearity of the materials with fixed high ε/σ filler contents at certain areas of the insulator.

Our research [11] focuses on the development of functionally graded materials (FGM) for GIS/GIL spacers where spatially graded dielectric permittivity (ε) and/or electrical conductivity (σ) is applied to the spacer bulk with the aim to reduce the locally high electric field by sharing the potential burden to the area with lower ε and/or σ. The incorporation of graded filler concentration into the base matrix material such as epoxy resin allows us to have graded ε/σ of the spacer bulk. It also enables us to control the electric field stress at several points at once, e.g. at the triple junctions of HV and GND side around GIS/GIL spacer. This ε/σ-FGM spacer can be fabricated by Flexible Mixture Casting (FMC) method as schematically illustrated in Fig. 1 [12]. This method allows us to fabricate a spacer model by mixing two different composites, each contains low and high ε/σ properties. The graded ε/σ can be created by controlling the mixing ratio of two composites with two syringe pumps and a static mixer.

In our past works, ε-FGM application to a 245 kV-class AC GIS cone-type spacer has been developed by FMC method, containing $SrTiO_3$ and $SiO_2$ fillers that bring about graded $\varepsilon_r$ between 10 and 4. Figs. 2 and 3 show the appearance of ε-FGM spacer as well as the flashover voltage under negative standard lightning impulse voltage, which are higher than that of conventional spacer by 28% at 0.6 MPa-abs of $SF_6$ gas pressure [13]. The application of both ε and σ graded materials (ε/σ-FGM) for HVDC GIS/GIL spacers has also been confirmed through electric field simulations, which reveals the effectiveness of U-type ε and grading-to-higher conductivity (GHC)-type σ distributions for electric field relaxation under various DC operating conditions [11].

This paper carries out the continuation and extension of our previous investigation, where the feasibility of ε/σ-FGM spacer is evaluated based on actual measured ε and σ characteristics of $SrTiO_3$-filled and SiC-filled epoxy composites, respectively. Toward the practical application of ε/σ-FGM spacer to HVDC GIS/GIL, electric field simulations are carried out to show the electrical performance of FGM spacers in σ-controlled resistive fields under DC steady state (DC-SS) and ε-controlled capacitive fields under lightning impulse (LI) voltage applications. The theoretical discharge inception voltage (TDIV) of ε/σ-FGM spacer is also calculated under LI voltage in comparison with the Uniform spacer with constant ε and σ.

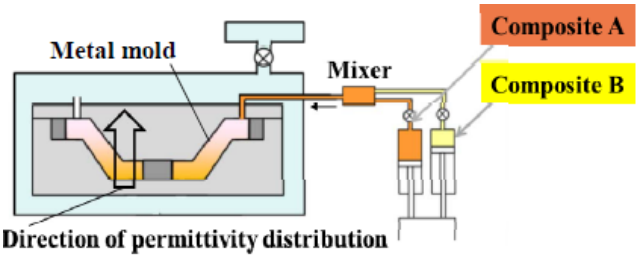


Fig. 1. FGM fabrication concept with FMC method [12].

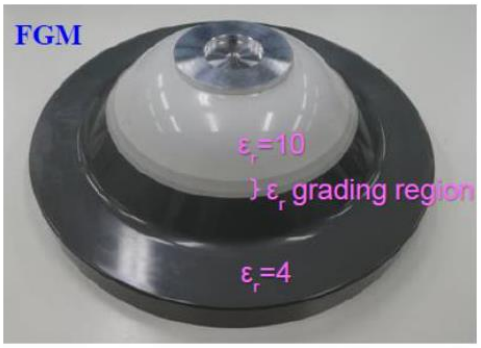


Fig. 2. 245 kV-class ε-FGM spacer sample [13].

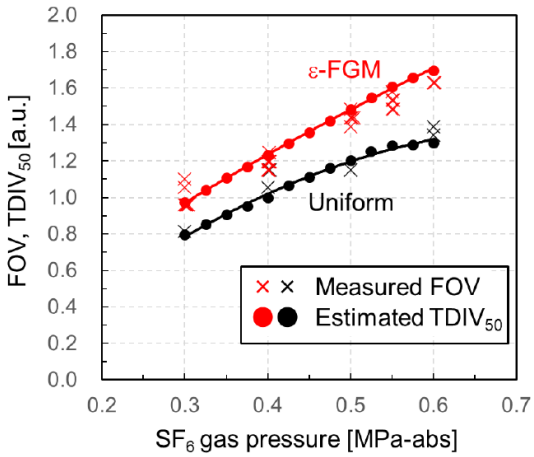


Fig. 3. Flashover voltage of 245 kV-class GIS spacer samples [13].

## II. ε AND σ CHARACTERISTICS OF SIC-FILLED EPOXY COMPOSITE

In order to investigate the effect of SiC filler contents to ε and σ characteristics, three types of $SiO_2$-filled epoxy-based bulk samples, each containing 0, 5, and 10 vol% SiC filler, are fabricated, where the total filler contents of SiC and $SiO_2$ is 50 vol% of the total epoxy-composite. Tables 1 and 2 show the material properties of the base epoxy resin and fillers.

### *A. ε Characteristics of SiC-filled Epoxy Composite*

The relative permittivity ($\varepsilon_r$) of each sample is measured through the capacitance measurements by LCR meter at various frequency. Fig. 4 shows $\varepsilon_r$ measurement results of each sample at the frequency of 1 kHz, as well as the curve fitting result

TABLE I
MATERIAL PROPERTIES OF EPOXY RESIN

| Base material | Specific gravity [g/ml] | Chemical structure |
|---|---|---|
| Epoxy | 1.17 | Bisphenol-A resin |
| Hardener | 1.21 | 3 or 4- methyl-1,2,3,6-tetrahydrophthalic anhydride |
| Hardening accelerator | 0.94 | 1-isobutil-2-methylimidazole |

TABLE II
SPECIFICATIONS OF FILLER PARTICLES

| Filler material | Specific gravity [g/ml] | Mean diameter [μm] |
|---|---|---|
| SiC | 3.16 | 3.71 |
| $SiO_2$ | 2.21 | 9.98 |
| $SrTiO_3$ | 5.13 | 1.00 – 1.50 |

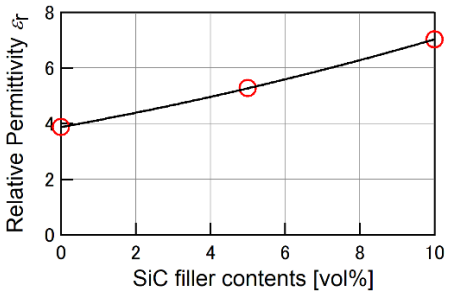


Fig. 4. $\varepsilon_r$ characteristics of SiC-filled epoxy composite.

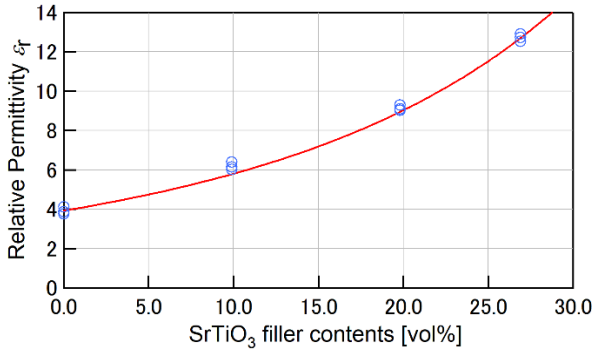


Fig. 5. $\varepsilon_r$ characteristics of $SrTiO_3$-filled epoxy composite [14].

indicated by the curve. The measured $\varepsilon_r$ of each 0, 5, and 10 vol% SiC-filled epoxy composite are 3.9, 5.3, and 7.0, respectively.

The $\varepsilon_r$ measurement results show relatively small difference in $\varepsilon_r$ between 0 vol% and 10 vol% SiC-filled epoxy composites ($\Delta\varepsilon_r \sim 3$), which is expected to be insufficient for effective electric field relaxation purpose under LI voltage. Thus, it is necessary to add another type of high $\varepsilon_r$ composite, so that we can create independently controlled ε and σ grading. In this ε/σ-FGM application, we adopt $\varepsilon_r$ characteristics of $SrTiO_3$-filled epoxy composite obtained from our past works on AC ε-FGM spacer, which applies ε grading from 12.7 to 4.0, as presented in Fig. 5 [14]. The specification of $SrTiO_3$ filler is included in Table 2.

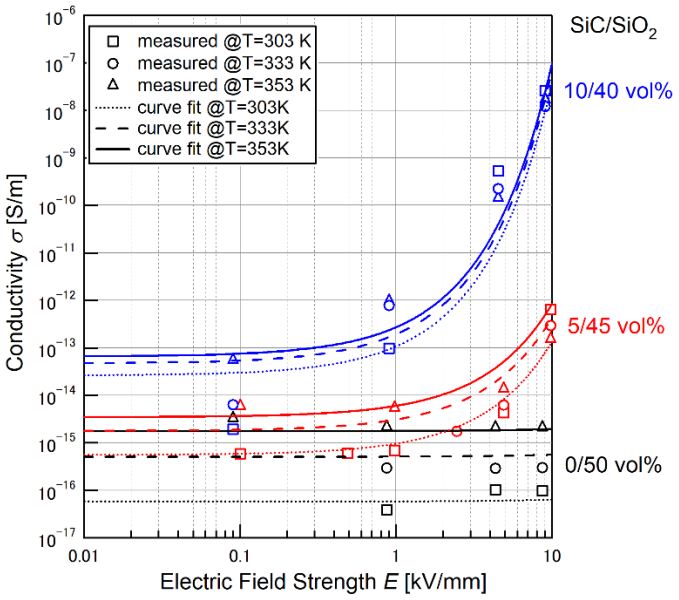


Fig. 6. σ characteristics of SiC-filled epoxy composite.

### B. σ Characteristics of SiC-filled Epoxy Composite

The conductivity (σ) of insulating materials is dependent on the temperature ($T$) and the electric field strength ($E$), which can be expressed by (1) [15-16],

$$\sigma(T,E) = \sigma_0 \exp\left(-\frac{W}{kT}\right)\exp(aE) \qquad (1)$$

where $\sigma_0$ is the specific conductivity constant in S/m, $k$ is the Boltzmann constant, and $W$ and $a$ are the temperature and electric field-dependency coefficients, respectively.

In order to comply with the equation, σ of each sample is measured using double-ring electrode system of JIS C 2170 under varying voltages at different temperatures according to IEC 62631-3-4. The markers in Fig. 6 show σ measurement results of 0 vol% (black), 5 vol% (red), and 10 vol% (blue) SiC-filled epoxy composites at 303 K, 333 K, and 353 K (different marker types). Multivariate analysis is then performed to the measurements' data and (1), which reveals the dependency of coefficients $\sigma_0$, $W$, and $a$ on SiC filler contents. The curves in Fig. 6 indicate the multivariate analysis results of σ characteristics as function of $T$, $E$, and SiC filler contents.

Based on the figure, adding SiC filler particles by 5 to 10 vol% can increase the basic σ level by about 10 to 100 times of non-SiC-filled epoxy composite. Furthermore, SiC-filled epoxy composite has higher electric field dependency which will further increase the σ at high electric field stress. On the contrary, the temperature dependency of SiC-filled epoxy composite decreases with SiC filler contents as well as with electric field. It is expected that SiC filler addition can bring an effective electric field relaxation despite temperature changes.

## III. ELECTRIC FIELD SIMULATION

### A. ε and σ Distributions of Scaled Model ε/σ-FGM Spacer

As discussed in the previous sections, it is important to have

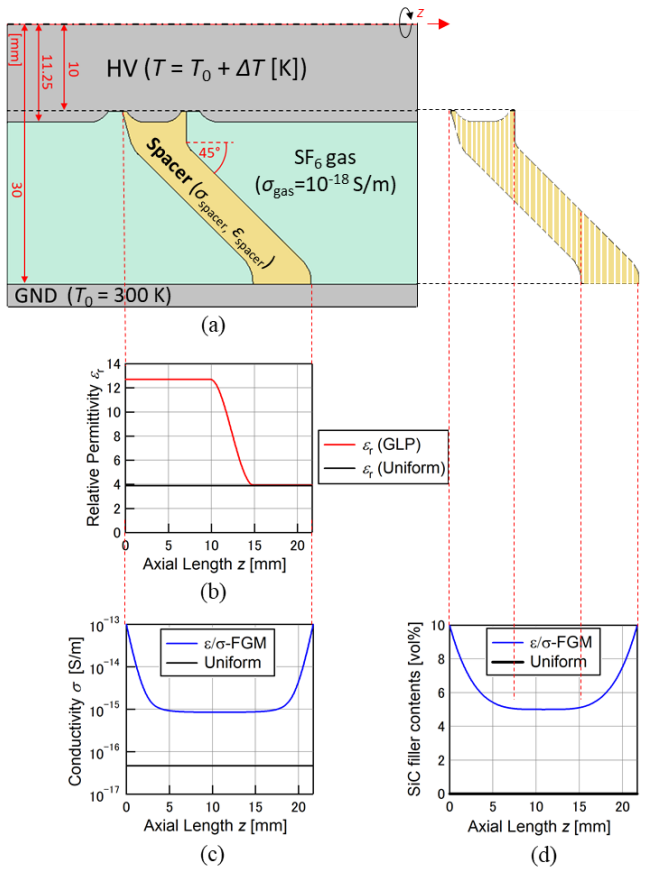


Fig. 7. (a) Scaled model of HVDC GIS spacer with (b) $\varepsilon_r$ distribution, (c) σ distribution (assuming $T$=300 K and $E$=1 kV/mm) and the respective (d) SiC filler contents distribution of ε/σ-FGM and the Uniform spacers.

both ε and σ distributions in DC GIS/GIL spacer with aim to reduce both capacitive and resistive fields under various DC operating conditions, such as DC-SS, DC-on, DC-polarity reversal (DC-PR), and superimposed (+/-) LI voltage on DC-SS [11]. For this purpose, ε characteristics of $SrTiO_3$-filled epoxy composite and σ characteristics of SiC-filled epoxy composite are implemented into a scaled model of ε/σ-FGM spacer for DC GIS, as shown in Fig. 7 (a).

The FMC fabrication method (Fig. 1) allows us to control ε and σ distributions independently, where grading to lower permittivity (GLP)-type ε distribution and U-shaped σ distribution are applied to ε/σ-FGM spacer, as illustrated in Figs. 7 (b) and (c), respectively. Fig. 7 (b) shows that $\varepsilon_r$ is graded from $\varepsilon_{r(max)}$ of 12.7 at the HV conductor/spacer interface, to $\varepsilon_{r(min)}$ of 4.0 at the GND/spacer interface [14]. The graded $\varepsilon_r$ is obtained from 0 to 26.9 vol% $SrTiO_3$-filled epoxy composite in Fig. 5. This $\varepsilon_r$ distribution is chosen in order to effectively suppress high electric field around the edge of shield electrode in the concave side owing to the higher $\varepsilon_r$ of the spacer around that area, where the potential burden is distributed toward the area with lower $\varepsilon_r$ near the GND tank. In this case, $\varepsilon_r$ characteristics of SiC-filled epoxy composite can be neglected, since it is smaller than that of $SrTiO_3$-filled epoxy composite.

Similarly, U-type σ distribution (Fig. 7 (c)) which is given by 5 to 10 vol% SiC-filled epoxy composite (Fig. 7 (d)) has the point of increasing σ of the spacer at the HV conductor/spacer interface, so that electric field is distributed more uniformly to the area with lower σ. However, in σ distribution, it is equally important to increase σ of the spacer at the GND/spacer interface, because with the presence of temperature distribution in the insulation medium, the equipotential lines are more likely to concentrate around the GND side. Keeping σ high at both ends of the spacer, i.e., U-type σ distribution will make the potential burden settled in the middle part of the spacer with lower σ. In this case, σ characteristics of $SrTiO_3$-filled epoxy composite are measured and confirmed to be less effective than those of SiC-filled epoxy composite, hence they are not taken into account in this electric field simulation.

The electric field simulation is conducted under two conditions: 27 kV DC-SS applied voltage and 100 $kV_{peak}$ LI applied voltage in order to investigate both σ-determined DC field and ε-determined AC field distributions. The DC-SS and LI voltage levels are chosen for the future fabrication and experimental verification of this scaled-model to correspond approximately to the electric field strength to that of 320 kV HVDC GIS spacer [11]. $E_{max}$ reduction effect given by ε/σ-FGM spacer is then monitored in comparison to that of the Uniform spacer with constant $\varepsilon_r$ and σ made of 0 vol% SiC and $SrTiO_3$-filled epoxy composites. Temperature ($T$) effect on electric field distribution is also investigated by implementing heat conduction analysis given by (2),

$$\nabla \cdot (\kappa \nabla T) = 0 \qquad (2)$$

with $\kappa$ is the thermal conductivity. $T$ of the HV conductor is varied from the lowest around room temperature of 300 K to the possible maximum $T$ in GIS during operation, which is 370 K [15], while $T$ of the GND conductor is kept at 300 K ($T_0$), so that $\Delta T$ ranges from 0 to 70 K.

### *B. Electric Field Grading Under DC-SS*

Fig. 8 shows the electric field distribution around (a) the Uniform spacer and (b) ε/σ-FGM spacer under 27 kV DC-SS, at $\Delta T$ of 0 K, 40 K, and 70 K. The maximum electric field strength ($E_{max}$) in $SF_6$ gas is indicated by the black dot in the figures.

As shown in the figure, electric field distribution around the Uniform spacer significantly changes with $\Delta T$, which is consistent with higher T-dependent σ characteristics at 0 vol% SiC-filled epoxy composite in Fig. 4. As $\Delta T$ increases, more volume of the Uniform spacer near the HV side has enhanced σ, causing potential burden pushed toward the spacer part near the GND side with lower σ (Fig. 8 (a)). However, ε/σ-FGM spacer has higher σ at the spacer part near the HV conductor, hence $E_{max}$ location appears in the middle part on the spacer's convex surface with lower σ. As σ distribution in this ε/σ-FGM spacer is composed of 5 to 10 vol% SiC-filled epoxy composite, even the middle part of the spacer has higher σ than the Uniform spacer (Fig. 7 (c)). Consequently, $E_{max}$ location does not change even when $\Delta T$ increases (Fig. 8 (b)). It is also consistent with the smaller T-dependency characteristics of 5 and 10 vol% SiC-

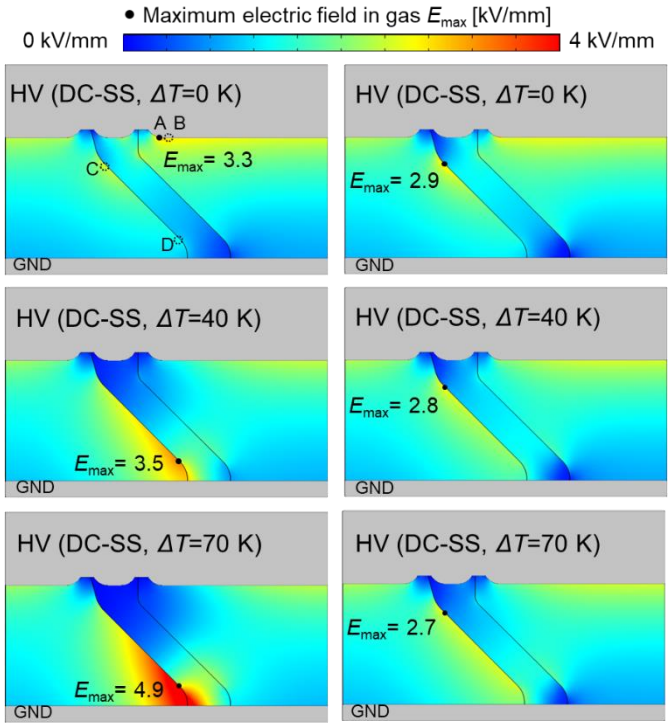


Fig. 8. Electric field distribution around (a) Uniform and (b) ε/σ-FGM spacers under 27 kV DC-SS at $\Delta T$=0, 40, and 70 K.

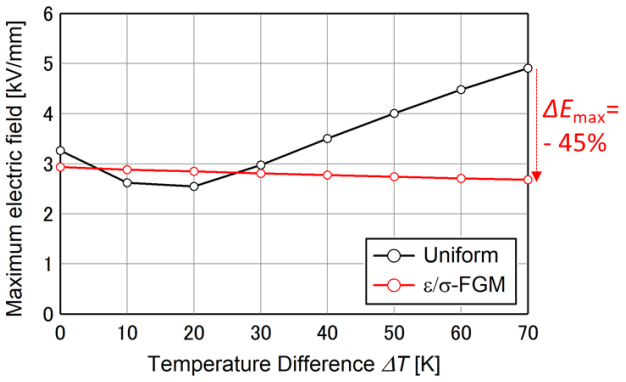


Fig. 9. $E_{max}$ in gas under DC-SS with varying $\Delta T$.

filled epoxy composites.

The trend of $E_{max}$ in gas against $\Delta T$ from 0 to 70 K for the Uniform and ε/σ-FGM spacers under DC-SS is described in Fig. 9. $E_{max}$ of the Uniform spacer first decreases at $\Delta T$=0 to 20 K, but then gradually increases at $\Delta T$=30 to 70 K. The first decline is caused by the temperature rise around the HV conductor/spacer interface that enhances σ of the spacer there, causing $E_{max}$ location on the shield edge at $\Delta T$=0 K (point A in Fig. 8 (a)) to be slightly pushed aside from the shield edge at $\Delta T$=10 K (point B in Fig. 8 (a)), and pushed away onto the curved area of the spacer's convex surface at $\Delta T$=20 K (point C in Fig. 8 (a)). As the electric field strength declines with increased distance from the HV conductor, $E_{max}$ around the Uniform spacer at $\Delta T$=10 to 20 K is smaller than that at $\Delta T$=0

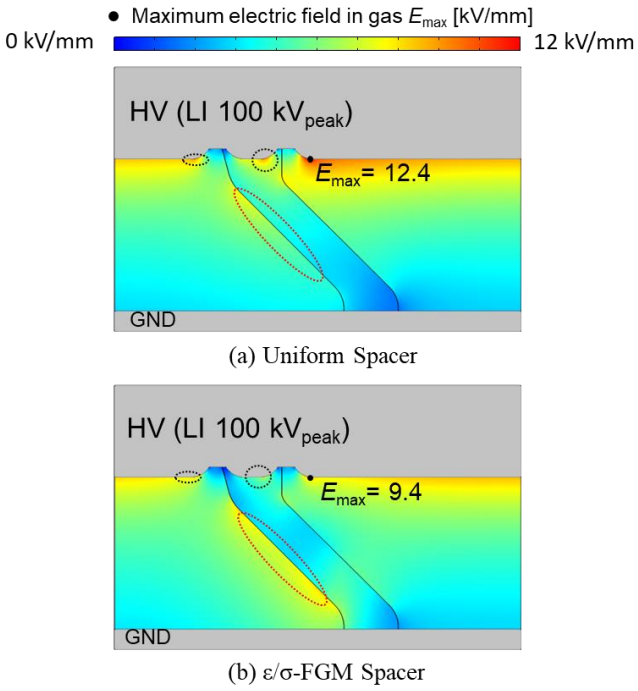


Fig. 10. *Electric field distribution around (a) Uniform and (b) ε/σ-FGM spacers at the peak of LI applied voltage.*

K. Then, $E_{max}$ location is shifted to point D near the GND/spacer interface with increasing magnitude as $\Delta T$ increases from 30 K to 70 K.

The figure also suggests almost constant suppression of $E_{max}$ around ε/σ-FGM spacer due to high σ given by 5 to 10 vol% SiC-filled epoxy composite which at the same time has smaller T-dependency. The largest $E_{max}$ reduction obtained under DC-SS is 45% at $\Delta T$=70 K.

### C. Electric Field Grading Under LI Voltage

The electric field distribution images in Fig. 10 are obtained through time-dependent electric field simulation under 100 $kV_{peak}$ LI voltage without temperature gap. As can be seen in Fig. 10, $E_{max}$ is found at the shield edge in the concave side for both of the Uniform and ε/σ-FGM spacers. However, the magnitude of $E_{max}$ of ε/σ-FGM spacer is reduced by 25% compared to that of the Uniform spacer.

Under 100 $kV_{peak}$ LI voltage, the capacitive fields are dominant, hence ε distribution within the spacer influences the electric field distribution. The constantly low ε distribution ($\varepsilon_r$ = 4) of the Uniform spacer has higher electric field strength around the shield edge in the concave side of the spacer (indicated by red area in Fig. 10 (a)). On the other hand, ε/σ-FGM spacer has higher ε from the spacer/HV conductor interface until the middle part of the spacer ($\varepsilon_r$ = 12.7). Thus, $E_{max}$ at the shield edge is reduced, and the area with higher electric field strength on the spacer's concave surface (indicated by red ellipse) shows that potential burden is distributed uniformly around the middle part of the spacer.

Fig. 11 shows time varying $E_{max}$ in $SF_6$ gas under LI 100 $kV_{peak}$, around the spacers without ε/σ grading (Uniform), with

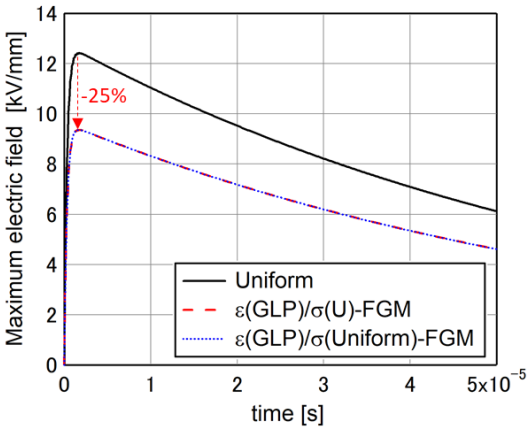


Fig. 11. *$E_{max}$ in $SF_6$ gas around the Uniform and ε(GLP)-FGM spacers with and without σ grading under LI 100 $kV_{peak}$.*

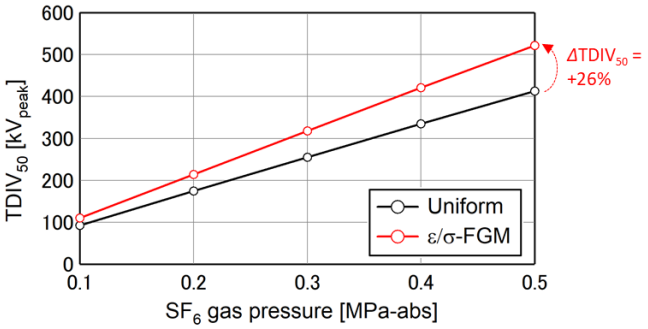


Fig. 12. *$TDIV_{50}$ of the Uniform and ε/σ-FGM spacers under LI voltage and at varying $SF_6$ gas pressure.*

only GLP-type ε grading (ε(GLP)/σ(Uniform)-FGM), and with GLP-type ε grading combined with U-type σ grading (ε(GLP)/σ(U)-FGM, Fig. 7). The graph reveals that $E_{max}$ around ε(GLP)/σ(Uniform)-FGM and ε(GLP)/σ(U)-FGM spacers are the same, confirming that the 25% $E_{max}$ reduction effect under LI voltage is due to the ε grading. In this case, there is no temperature dependence on $E_{max}$.

## IV. $TDIV_{50}$ Calculation

### A. $TDIV_{50}$ Calculation by Volume-Time Theory

Breakdown test is an ultimate method to evaluate performances of the insulating materials. The electric field relaxation effect of ε/σ-FGM spacer which has been disclosed through simulation should contribute to the breakdown voltage improvement. The Volume-Time theory allows us to calculate the discharge inception probability at a given applied voltage which is suggested by the generation of initial electrons in high electric field volume in $SF_6$ gas, as expressed in (3) [12],

$$P = 1 - \exp\left[-\int_t \int_{V_{cr}} \frac{dn_e}{dt}\left(1-\frac{n}{\alpha}\right) dV dt\right] \quad (3)$$

where $P$ is the generation probability of initial electrons, $dn_e/dt$ is the number of electrons desorbed from $SF_6$- ions per unit time and per unit volume, $\alpha$ and $\eta$ are the ionization and attachment coefficients. $V_{cr}$ is the critical volume which satisfies a condition where $\alpha > \eta$ and when streamer is formed, according to Schumann's formula, as in (4),

$$\int_{x_{cr}} (\alpha - \eta)\, dx = K \quad (4)$$

where $K$ equals 18 for $SF_6$ gas and $x_{cr}$ is the critical path along electric lines of force. The term $(\alpha - \eta)$ for $SF_6$ gas is expressed in (5),

$$\frac{\alpha-\eta}{p} = 27\left(\frac{E}{p} - 87.75\right) \quad (5)$$

where $E$ is the electric field strength in kV/mm and $p$ is the absolute pressure of $SF_6$ gas in MPa.

### B. $TDIV_{50}$ Calculation Results

$TDIV_{50}$ refers to the applied voltage level at which the probability (P) of the discharge inception in (3) is 50%. Here, $TDIV_{50}$ is calculated under standard LI voltage at varying $SF_6$ gas pressure from 0.1 to 0.5 MPa-abs, with results as presented in Fig. 12. The graph shows $TDIV_{50}$ improvement of ε/σ-FGM spacer by at least 19% at 0.1 MPa-abs and at most 26% at 0.5 MPa-abs, compared to the Uniform spacer. This TDIV improvement is achieved due to the electric field relaxation effect which is contributed by ε grading, rather than σ grading, because mainly capacitive fields exist under time-varying LI voltage, as described in Fig. 11. With these results, it is verified that ε/σ-FGM spacer with GLP-type ε distribution and U-type σ distribution can give electric field relaxation effect, and hence TDIV improvement in DC GIS insulation system.

## V. Conclusion

This paper confirmed that $SrTiO_3$-filled and SiC-filled epoxy composites with independent ε and σ grading are applicable to ε/σ-FGM spacers for DC GIS/GIL. The electric field as well as TDIV calculation results have confirmed the following points.

1. σ profiles as functions of $T$, $E$, and SiC filler contents were measured and their database was constructed by multivariate analysis.
2. ε/σ-FGM spacer with GLP-type ε distribution ($\varepsilon_r$=12.7 to 4) containing 0 to 26.9 vol% $SrTiO_3$-filled epoxy composite and U-shaped σ distribution (σ=$10^{-15}$ to $10^{-7}$ S/m) containing 5 to 10 vol% SiC-filled epoxy composite can give $E_{max}$ reduction under 27 kV DC-SS and 100 $kV_{peak}$ LI voltage by at most 45% (at $\Delta T$=70 K) and 25%, respectively. Moreover, $TDIV_{50}$ under LI applied voltage can be improved by 19 to 26% at $SF_6$ gas pressure of 0.1 to 0.5 MPa-abs, compared to the Uniform spacer.
3. σ(U) distribution in ε/σ-FGM spacer contributes to the reduction of resistive fields under DC-SS. The high σ given by 5 to 10 vol% SiC-filled epoxy composite has smaller T-dependence, allowing almost constant field relaxation despite the increase in the temperature.
4. ε(GLP) distribution in ε/σ-FGM spacer contributes to the reduction of capacitive fields under LI applied voltages, hence $TDIV_{50}$ is improved.

The feasibility of ε/σ-FGM application to HVDC GIS/GIL spacer has been analytically investigated with promising results. The ε/σ distribution specified in this paper is one example which is effective for electric field relaxation. The ε/σ distribution shapes may change depending on the size and shape of DC GIS/GIL spacer and can be optimized through inverse analysis [17]. Application of ε/σ-FGM spacers to AC or DC GIS/GIL with $SF_6$ gas alternatives can also be expected. Experimental verification by fabrication of ε/σ-FGM spacer samples and their breakdown tests including long-term characteristics will be our future works.

## REFERENCES

[1] C. Li *et al*, "Novel HVDC spacers by adaptive controlling surface charges – Part I: charge transport and control strategy," *IEEE Trans. Dielectr. Electr. Insul.,* vol. 25, no. 4, pp. 1238–1245, Aug. 2018, doi: 10.1109/TDEI.2018.007054.

[2] W. Li, X. Li, B. Guo, C. Wang, Z. Liu, and G. Zhang, "Topology optimization of truncated cone insulator with graded permittivity using variable density method," *IEEE Trans. Dielectr. Electr. Insul.*, vol. 26, no. 1, pp. 1–8, Feb. 2019, doi: 10.1109/TDEI.2018.007315.

[3] B. X. Du, H. C. Liang, and J. Li, "Surface coating affecting charge distribution and flashover voltage of cone-type insulator under DC stress," *IEEE Trans. Dielectr. Electr. Insul.*, vol. 26, no. 3, pp. 706–713, Jun. 2019. doi: 10.1109/TDEI.2018.007616.

[4] N. Zebouchi, H. Li, and M. A. Haddad, "Development of future compact and eco-friendly HVDC gas-insulated systems: shape optimization of a DC spacer model and novel materials investigation," *Energies*, vol.13, no.3288, pp. 1-14, Jun 2020, doi: 10.3390/en13123288.

[5] CIGRE WG D1.56, "Field grading in electrical insulation systems," *CIGRE Technical Brochure*, no. 794, 2020. Available: https://e-cigre.org/publication/794-field-grading-in-electrical-insulation-systems

[6] M. Pradhan, H. Greijer, G. Eriksson, and M. Unge, "Functional behaviours of electric field grading composite materials*," IEEE Trans. Dielectr. Electr. Insul.*, vol. 23, no. 2, pp. 768-778, Apr. 2016, doi:10.1109/TDEI.2015.005288.

[7] B. X. Du, H. C. Liang, and J. Li, "Novel spacer coated with functionally graded ZnO film for HVDC gas insulated line," *IEEE Trans. Dielectr. Electr. Insul.*, vol.27, no. 1, pp. 231-239, Feb. 2020, doi: 10.1109/TDEI.2019.008396.

[8] X. Li *et al*, "3D printing fabrication of conductivity non-uniform insulator for surface flashover mitigation." *IEEE Trans. Dielectr. Electr. Insul.*, vol. 26, no. 4, pp. 1172-1180, Aug. 2019, doi: 10.1109/TDEI.2019.007938.

[9] C. Li *et al*, "Novel HVDC spacers by adaptively controlling surface charges – Part II: Experiment," *IEEE Trans. Dielectr. Electr. Insul.*, vol. 25, no. 4, pp. 1248-1258, Aug. 2018, doi: 10.1109/TDEI.2018.007056.

[10] H. Yin, W. Li, Y. Zhang, C. Wang, Z. Jiang, and G. Zhang, "Characterization of polypropylene/titanium dioxide composites used for 3D printing of dielectric functionally graded insulators," presented at the 22nd Int. Symp. High Voltage Engineering (ISH), no. 947, Nov. 21-25, 2021. [Online].

[11] Rachmawati, H. Kojima, N. Hayakawa, K. Kato, and N. Zebouchi, "Electric field simulation of permittivity and conductivity graded materials (ε/σ-FGM) for HVDC GIS spacers," *IEEE Trans. Dielectr. Electr. Insul.*, vol. 28, no. 2, pp. 736–744, Apr. 2021, doi: 10.1109/TDEI.2020.009343.

[12] N. Hayakawa, Y. Miyaji, H. Kojima, and K. Kato, "Simulation on discharge inception voltage improvement of GIS spacer with permittivity graded materials (ε-FGM) using Flexible Mixture Casting method," *IEEE Trans. Dielectr. Electr. Insul.*, vol. 25, no. 4, pp. 1318–1323, Aug. 2018, doi: 10.1109/TDEI.2018.007236.

[13] N. Hayakawa *et al*, "Flashover voltage estimation of cone-type GIS spacer with permittivity graded materials (ε-FGM) by Volume-Time theory in consideration with conductor surface roughness $SF_6$ gas," presented at the 22nd Int. Symp. High Voltage Engineering (ISH), no. 705, Nov. 21-25, 2021. [Online].

[14] Y. Miyazaki *et al*, "Breakdown characteristics of cone-type ε-FGM spacer for gas insulated switchgears," *IEE Japan-A*, vol. 141, no. 10, pp. 546-551, 2021, doi: 10.1541/ieejfms.141.546.

[15] M. Hering, S. Grossmann, J. Speck, and U. Riechert, "Investigation of the temperature influence on the breakdown voltage in gas insulated systems under DC voltage stress," in *Proc. 18th Int. Symp. High Voltage Engineering (ISH)*, Seoul, South Korea, 2013, pp.1354-1359.

[16] H. Li, N. Zebouchi, and A. Haddad, "Theoretical and practical investigations of spacer models for future HVDC GIL/GIS applications," in *Proc. 21st Int. Symp. High Voltage Engineering (ISH)*, vol. 2, Budapest, Hungary, 2019, pp. 1538-1549.

[17] K. Kato *et al*, "Inverse analysis of optimum permittivity distribution for FGM spacer in consideration with multiple objective functions in gaseous insulation systems," presented at the *22nd Int. Symp. High Voltage Engineering (ISH)*, no. 401, Nov. 21-25, 2021. [Online].

**Rachmawati** was born in Indonesia in 1988. She received the B.Sc. degree and M. Eng degree both in electrical engineering from Bandung Institute of Technology, Indonesia in 2010 and Tohoku University, Japan, in 2013, respectively. She is currently a doctoral student in Graduate School of Engineering, Nagoya University, Japan.

She was an academic assistant in School of Engineering and Informatics (SEEI), Bandung Institute of Technology, from 2017 to 2019.

Ms. Rachmawati is a student member of IEE of Japan and CIGRE.

**Hiroki Kojima** (Member, IEEE) was born in Japan, in 1975. He received his Ph.D degree in 2004 in energy engineering and science from Nagoya University, Japan.

He was a Research Fellow of the Japan Society for the Promotion of Science from 2000 to 2003. Since 2004, he has been at Nagoya University and presently he is an Associate Professor of Nagoya University in the Department of Electrical Engineering.

Dr. Kojima is a senior member of IEE of Japan.

**Naoki Hayakawa** (Member, IEEE) was born in Japan, in 1962. He received his Ph.D degree in 1991 in electrical engineering from Nagoya University, Japan.

He has been at Nagoya University since 1990, where he is presently a Professor in the Department of Electrical Engineering. From 2001 to 2002, he was a guest scientist at the Forschungszentrum Karlsruhe, Germany.

Prof. Hayakawa is a member of IEE of Japan and CIGRE.

**Katsumi Kato** was born in 1969. He received his Ph.D degree in 1997 in electrical engineering from Nagoya University, Japan.

From 1997, he was on the faculty of Nagoya University. Currently he is an Associate Professor at the National Institute of Technology, Niihama College, Japan, in the Department of Electrical Engineering and Information Science.

Dr. Kato is a member of IEE of Japan.

**Nabila Zebouchi** received the PhD. degree in electrical engineering from the University Paul Sabatier, Toulouse, France, in 1997.

She has worked at ABB AB Corporate Research in Sweden, at the French company Nexans manufacturer of high voltage cables and accessories and the Belgian Ceramic Research Centre. She participated as a full member from 2013 to 2019 to the CIGRE working group D1-56 dealing with Field Grading in Electrical Insulation Systems. She is presently working on FLEXIS Project-WP 16: Environmentally Friendly Electrical Power Plant and Insulation, at the Advanced High Voltage Engineering Research Centre, Cardiff University, UK.